Distribution and lateral mobility of DC-SIGN on immature dendritic cells – implications for pathogen uptake

Aaron K. Neumann[1,2], Nancy L. Thompson[3] and Ken Jacobson[1,2,*]

[1]Department of Cell and Developmental Biology, [2]Lineberger Comprehensive Cancer Center and [3]Department of Chemistry, University of North Carolina at Chapel Hill, Chapel Hill, NC 27599, USA

*Author for correspondence (e-mail: frap@med.unc.edu)

Accepted 19 November 2007
Journal of Cell Science 121, 634-643 Published by The Company of Biologists 2008
doi:10.1242/jcs.022418

Summary

The receptor C-type lectin DC-SIGN (CD209) is expressed by immature dendritic cells, functioning as an antigen capture receptor and cell adhesion molecule. Various microbes, including HIV-1, can exploit binding to DC-SIGN to gain entry to dendritic cells. DC-SIGN forms discrete nanoscale clusters on immature dendritic cells that are thought to be important for viral binding. We confirmed that these DC-SIGN clusters also exist both in live dendritic cells and in cell lines that ectopically express DC-SIGN. Moreover, DC-SIGN has an unusual polarized lateral distribution in the plasma membrane of dendritic cells and other cells: the receptor is preferentially localized to the leading edge of the dendritic cell lamellipod and largely excluded from the ventral plasma membrane. Colocalization of DC-SIGN clusters with endocytic activity demonstrated that surface DC-SIGN clusters are enriched near the leading edge, whereas endocytosis of these clusters occurred preferentially at lamellar sites posterior to the leading edge. Therefore, we predicted that DC-SIGN clusters move from the leading edge to zones of internalization. Two modes of lateral mobility were evident from the trajectories of DC-SIGN clusters at the leading edge, directed and non-directed mobility. Clusters with directed mobility moved in a highly linear fashion from the leading edge to rearward locations in the lamella at remarkably high velocity (1420±260 nm/second). Based on these data, we propose that DC-SIGN clusters move from the leading edge – where the dendritic cell is likely to encounter pathogens in tissue – to a medial lamellar site where clusters enter the cell via endocytosis. Immature dendritic cells may acquire and internalize HIV and other pathogens by this process.

Supplementary material available online at
http://jcs.biologists.org/cgi/content/full/121/5/634/DC1

Key words: CD209, DC-SIGN, Endocytosis, Microdomain, Plasma membrane, Protein cluster

Introduction

Immature dendritic cells express many antigen-capture receptors, including those of the C-type lectin family, and are highly endocytic. These characteristics enable immature dendritic cells to bind and internalize antigen efficiently (Banchereau and Steinman, 1998; Weis et al., 1998). Some pathogens, such as HIV-1, can exploit the mechanisms of immature dendritic cells for antigen acquisition and internalization to enhance their infectivity while avoiding lysosomal degradation.

The surfaces of numerous virions, bacteria, yeast and parasite species present glycoproteins with affinity for DC-SIGN, so DC-SIGN is a pattern-recognition receptor for microbial surfaces (Cambi et al., 2005). Studies using transmission EM and near-field scanning optical microscopy (NSOM) have demonstrated that DC-SIGN on the surface of fixed immature dendritic cells is arranged into distinct nanoscale clusters (Cambi et al., 2004; Koopman et al., 2004). Clustering of DC-SIGN is thought to improve binding to small, multivalent ligands, such as a viral particle or a bacterium, by providing high-avidity-binding platforms. Both avidity and affinity of pathogen interactions with DC-SIGN are likely to be important for efficient capture of particles that present only a very small binding surface for contact with the immature DC.

HIV-1 is a significant human pathogen that binds to DC-SIGN to promote infection. In the classical HIV-1 infection pathway, the virion binds to CD4 and chemokine receptor, leading to fusion of the virion envelope and cellular membrane (Frankel and Young, 1998; Ray and Doms, 2006). By contrast, binding to DC-SIGN leads to non-fusogenic uptake of virions by immature dendritic cells (Geijtenbeek et al., 2000; Kwon et al., 2002). Moreover, these internalized virions can be later delivered to target T cells through cell-cell contacts or 'virological synapses'. This process is termed 'infection in trans' and is thought to lead to an enhanced infection of $CD4^+$ T cells by prolonging virion infectivity and promoting an efficient exposure of target T cells to HIV-1 (Geijtenbeek et al., 2002; Wu and KewalRamani, 2006).

Binding and internalization represent the first obstacles that a virus must overcome to achieve infection, and live cell imaging studies of virus-cell interactions have elucidated cell biology of the very earliest phases in the infection processes of other enveloped viruses. For instance, several recent reports on murine leukemia virus (MLV) and influenza A have described the transport of these enveloped viruses laterally in the plasma membrane, providing important insights into these early milestones in viral infection (Lakadamyali et al., 2003; Lehmann et al., 2005). In this paper, we describe our findings regarding the distribution and dynamics of the HIV-1 receptor DC-SIGN in live cells, including immature dendritic cells. Moreover, we demonstrate that DC-SIGN translates in a directed fashion from

Journal of Cell Science

areas of concentration at the leading edge to mid-lamellar sites of internalization.

Results

Clustering of DC-SIGN in live cells

We have observed clusters of DC-SIGN as punctate immunofluorescence staining in fixed specimens of DC-SIGN-expressing cells. Such clusters were observed in a wide variety of cell types tested, including Raji (Raji-DCSIGN) or NIH 3T3 (MX-DCSIGN) stably expressing DC-SIGN, or immature monocyte-derived dendritic cells (MDDCs) (Fig. 1A-C). These cells were not subjected to any receptor ligation prior to fixation, so the observation of distinctly clustered DC-SIGN supports the conclusion that DC-SIGN forms clusters in the plasma membrane in the absence of ligation. However, to completely exclude the potential of fixation and/or staining artifacts, we imaged DC-SIGN in live cells using a monovalent reagent to prevent crosslinking of DC-SIGN. When labeled briefly with Alexa-Fluor-568-conjugated anti-DC-SIGN F(ab) and imaged immediately, clusters of DC-SIGN were evident upon the membranes of live Raji-DC-SIGN cells, MX-DCSIGN cells, and MDDCs (Fig. 1D-F). No staining was observed when the same labeling procedure was applied to parental Raji and NIH 3T3 lines (data not shown).

DC-SIGN cluster size distribution

Table 1 shows object-size results obtained from Gaussian fitting analyses for the five different image types and all retained peaks (see Materials and Methods). The data indicate that the average size of the DC-SIGN clusters is larger than ~500 nm and that the distribution of DC-SIGN cluster sizes is much broader than for the other object types.

The results for the quantum dots (assumed to be point particles) imply a point-spread-function width of s=108 nm, h=125±13 nm and a full-width half-maximum (FWHM) value of ~300 nm. By using this value, the FWHM values for the peaks produced by the 216-nm and 431-nm diameter beads were predicted by calculating the implied fluorescence as a function of x, with y=0, as:

$$F(x) \propto \int_{-r}^{r} \sqrt{r^2-\xi^2}\,\exp\left[-\frac{(x-\xi)^2}{2s^2}\right]d\xi \ , \qquad (1)$$

where r=108 nm or 215.5 nm, respectively. The predicted fluorescence values were fit to Equation 5 with d=0, j=c and i=x. These fits implied FWHM values for the two bead types of 328 nm and 408 nm, respectively. These values are considerable lower than the measured values shown in Table 1 (by about 30-50%). The reason for this discrepancy is not known. Two possible explanations are that the beads were not firmly adhered to the surface and underwent considerable 'wobble' during image acquisition, and that the beads, once adhered, were not truly spherical but spread into more of a ellipsoidal shape with a larger diameter. Nonetheless, the agreement between the predicted and observed FWHM values is reasonably good.

For further analysis, the histogram of FWHM values for DC-SIGN clusters was examined. Extreme FWHM values of less than 300 nm (see above) or greater than 1400 nm were omitted from further analysis, reducing the total number of included clusters from 848 to 804 (i.e. rejecting 5% or the previously retained peaks). The result is shown in supplementary material Fig. S1A. To convert the measured DC-SIGN FWHM values to cluster diameters, simulations were carried out in which the fluorescence as a function of x, with y=0, for a uniformly fluorescent circle of radius r and diameter w=2r was calculated as:

$$F(x) \propto \int_{-r}^{r} \exp\left[-\frac{(x-\xi)^2}{2s^2}\right]d\xi = s\sqrt{\frac{\pi}{2}}\left[erf\left(\frac{x+r}{s\sqrt{2}}\right) - erf\left(\frac{x-r}{s\sqrt{2}}\right)\right], \qquad (2)$$

with x in nm and s=125 nm. The predicted values of F(x) were fit to Equation 5 with d=0, j=c and i=x, to give values of h, which were converted to FWHM values. The supplementary material Fig. S1B shows the results of these simulations as well as the best-fit to the empirical function:

$$FWHM\ (\text{nm}) = 300\ \text{nm} + \alpha w + \beta w^2 \ . \qquad (3)$$

The best-fit values of the free parameters were α=0.273 and β=0.000291 nm^{-1}. DC-SIGN cluster diameters w were thus calculated as:

$$w = \frac{-\alpha + \sqrt{\alpha^2 + 4\beta\,[FWHM(\text{nm}) - 300\ \text{nm}]}}{2\beta} \ . \qquad (4)$$

The results, as shown in Fig. 1G, indicate a median diameter for DC-SIGN clusters of 615 nm with a large standard deviation (s.d.) of 269 nm.

DC-SIGN-cluster photobleaching and recovery

We performed fluorescence recovery after photobleaching (FRAP) measurements in live cells on individual F(ab) labeled DC-SIGN domains to determine their stability. The rate of DC-SIGN exchange between the domains and surrounding membrane reflects the mechanism underlying the observed clustering of DC-SIGN (i.e. permanent anchorage in clusters versus partitioning between domain bound and unbound pools). Using a confocal microscope, one or a few clusters were partially bleached and the remaining fluorescence was used to track the affected cluster, and measure its recovery over time (Fig. 2A,C). FRAP curves for DC-SIGN clusters on live MX-DCSIGN cells and dendritic cells showed remarkably little recovery (Fig. 2B,D). Mobile fractions from all cluster FRAP data showed that generally <10% of the DC-SIGN within a cluster exchanges with the surrounding membrane.

Table 1. Gaussian fits of DC-SIGN cluster size distribution

Image type	h (pixels)	FWHM (nm)	Number of images	Number of peaks
DC-SIGN	2.24±1.16	580±300	2	848
quantum dots	1.16±0.12	301±32	3	1241
216-nm beads	1.88±0.11	487±29	5	2773
431-nm beads	2.06±0.13	535±33	5	216
216-nm-bead aggregates	3.69±0.91	956±237	1	22

Values are given as median ± s.d. Values for full-width half-maximum (FWHM) diameters were calculated as the product of 2.4×h×108 nm. h, peak width.

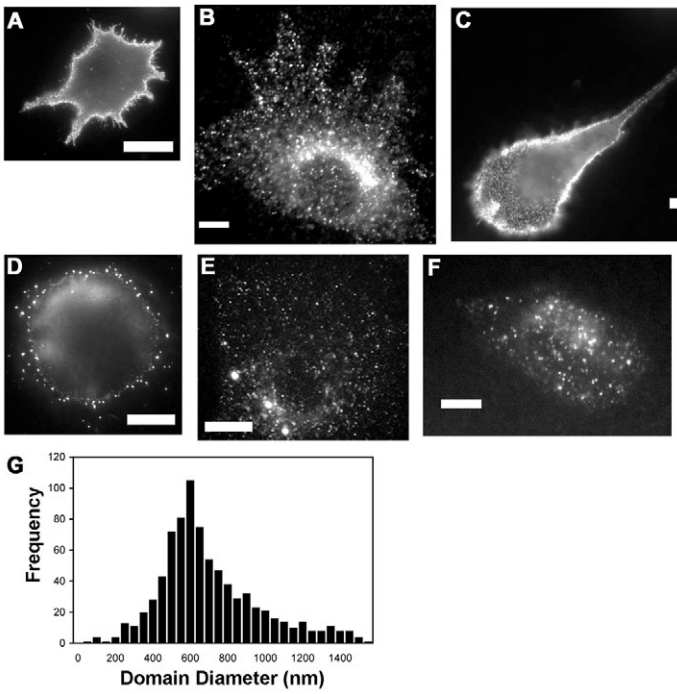

Fig. 1. (A-C) DC-SIGN staining (DCN46 mAb) in fixed cells shown for (A) fibronectin-adhered Raji-DCSIGN cells, (B) MX-DCSIGN cells and (C) MDDCs. (D-E) DC-SIGN staining in live cells using Alexa-Fluor-568-conjugated anti-DC-SIGN F(ab) shown for (D) Raji-DC-SIGN cells, (E) MX-DCSIGN cells, (F) MDDCs. All images were focused on the dorsal surface. Scale bars, 10 μm. (G) Distribution of DC-SIGN cluster sizes on MX-DCSIGN cells (n=804).

Polarized lateral distribution of DC-SIGN

We examined DC-SIGN distribution on the ventral membranes of Raji-DCSIGN cells and MDDCs. Cells that had firmly attached to the substrate were illuminated by total internal reflection (TIR) optics to provide a thin optical section of the cell limited to the ventral cell surface within ~150 nm of the glass. In the case of Raji-DCSIGN cells, we observed a striking exclusion of DC-SIGN staining in the central area of the ventral membrane (Fig. 3A). We performed controls for possible optical or staining artifacts. A highly arched ventral membrane might cause selective TIR excitation of peripheral fluorophores. Imaging Raji-DCSIGN cells with a lipophilic dye, DiI, which evenly stains the bilayer, revealed that the entire ventral membrane surface is evenly accessible to the TIR field (Fig. 3B). Also, peripheral tight contacts might limit diffusion to the space underneath the cell and prevent efficient antibody staining of the ventral membrane. We applied high molecular weight dextran (580 kDa) conjugated to fluorescein and measured the green fluorescence intensity by TIR in a region underneath an unlabeled Raji-DCSIGN cell both before and after addition of fluorescein-dextran. We observed a dramatic increase in ventral surface fluorescence intensity occurring immediately after addition of fluorescein-dextran, indicating that macromolecules have access to the ventral surface (Fig. 3C). Furthermore, we were able to visualize the ventral staining of other membrane proteins such as CD46 and CD59 by TIRF microscopy, and these antigens did not exhibit ventral membrane exclusion similar to DC-SIGN (Fig. 3D). We also observed the ventral plasma membranes of immature DC to determine if a similar protein distribution occurs in these cells. Immature MDDCs stained for DC-SIGN exhibit a paucity of DC-SIGN staining on the central region of the ventral lamellar surface although the degree of exclusion appears somewhat less in DC than in Raji-DCSIGN cells (Fig. 3E).

To investigate the dorsal membrane distribution of DC-SIGN, we acquired z-series stacks (200-nm steps) of epifluorescence images and subjected them to deconvolution to remove out-of-focus light. Whereas DC-SIGN is markedly absent from the ventral membrane on Raji-DCSIGN cells, clusters of DC-SIGN covered the dorsolateral membrane surfaces of these cells (Fig. 3F and supplementary material Movie 1). Dendritic cells have a polarized morphology and a dynamic leading edge (i.e. membrane ruffling) (Burns et al., 2004; van Helden et al., 2006); therefore, we hypothesized that the dorsal membrane distribution of this important antigen receptor may also be polarized towards the dynamic edges of the dendritic cell. Indeed, in immature dendritic cells, DC-SIGN imaged upon the dorsal lamellar membrane (focused 2 μm above the glass) revealed a band of bright staining just behind the leading edge (Fig. 3G). Three-dimensional projections of deconvoluted z-series stacks from immature dendritic cells demonstrate that there is an accumulation of DC-SIGN near the edges of the lamellipod, and this concentration is especially prominent in areas with membrane ruffles, as observed in DIC images of the same cell (Fig. 3H and supplementary material Movie 2). We co-stained dendritic cells for DC-SIGN and membrane content using DiI (supplementary material Fig. S2A,B) and normalized DC-SIGN signal to DiI fluorescence (supplementary material Fig. S2C). Peripheral areas apparently enriched in DC-SIGN persisted after normalization, demonstrating that they represent true accumulations of DC-SIGN near the leading edge of the cell. The averaged DC-SIGN-to-DiI ratio along regularly spaced radii from the perinuclear zone to the leading edge shows an overall enrichment of DC-SIGN of ~50% near the edge (supplementary material Fig. S2D,E). Student's t-test was applied to the mean ratios binned over pixels <3 μm from the edge versus pixels ⩾3 μm from the edge and showed that the enrichment of DC-SIGN <3 μm from the cell edge was highly significant ($P<10^{-9}$).

Endocytosis of DC-SIGN

The concentration of DC-SIGN at the leading edges suggested that the leading edge might be a prime site for antigen and pathogen acquisition. However, significant endocytosis of DC-SIGN clusters is unlikely to occur at the leading edge of immature dendritic cells because of the dense actin meshwork associated with protruding cell edges (Theriot and Mitchison, 1992) and because few vesicles are seen in DIC images of the leading edge of dendritic cells (Fig. 3H and data not shown). Therefore we hypothesized that DC-SIGN clusters require rearward transport from leading edge regions of DC-SIGN enrichment to zones of receptor internalization.

We identified sites of internalization of DC-SIGN by colocalization of DC-SIGN and a functional marker of endocytosis. Live immature dendritic cells were rapidly and concurrently stained with anti-DC-SIGN F(ab) conjugated to Alexa-Fluor-568 while bathed in 37°C culture medium containing BSA-fluorescein. Brief exposure to the F(ab) was sufficient to label surface-accessible DC-SIGN. FITC-BSA was sequestered within endocytic vesicles created during the staining period and remained as a marker of endocytic vesicles after thorough washout and fixation.

Journal of Cell Science

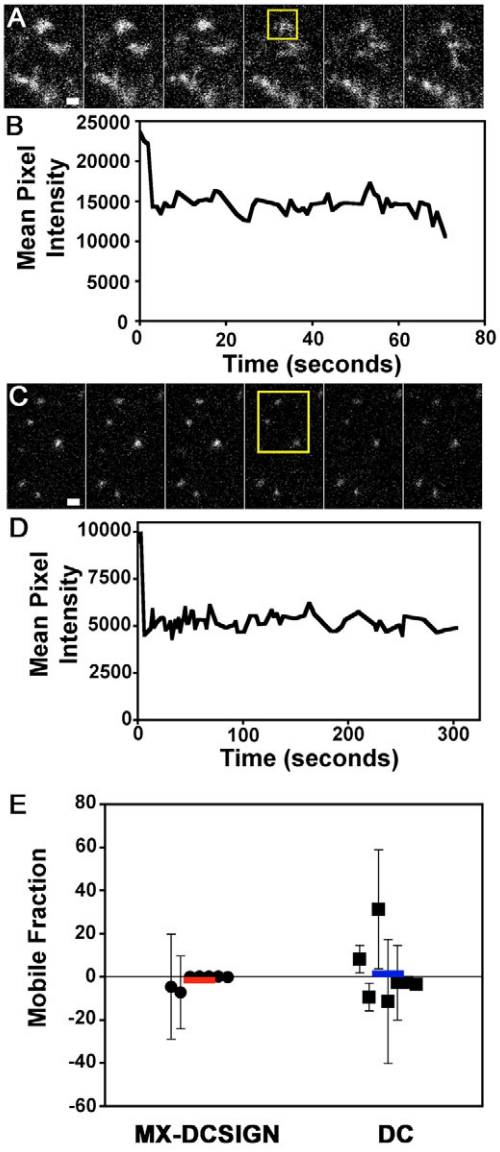

Fig. 2. DC-SIGN cluster photobleaching and recovery. (A) Montage showing the bleaching of a representative DC-SIGN cluster on an MX-DCSIGN cell stained with anti-DC-SIGN F(ab). The bleached region is indicated with a yellow box and bleaching occurred between the third and fourth frames. (B) The complete intensity profile in time of the bleached cluster. (C) A montage showing the bleaching of several DC-SIGN clusters on a dendritic cell. (D) Bleaching and recovery phase for a representative cluster on this dendritic cell. (E) Distribution of mobile fractions (M_f) as measured from the FRAP curves of all DC-SIGN clusters analyzed in both MX-DCSIGN cells and dendritic cells (n=7 in each cell type, error bars denote ± s.d.). Red and blue bars show the mean M_f for all trials per cell type. Scale bars, 1 μm.

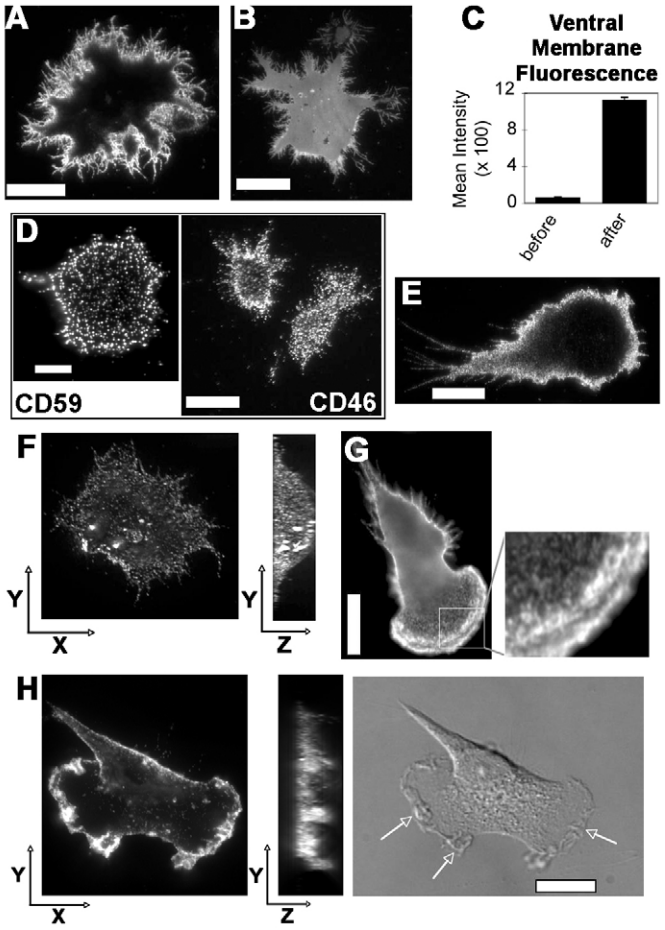

Fig. 3. (A) Raji-DCSIGN cells visualized by total internal reflectance (TIR) illumination of the ventral membrane after fixation and staining for DC-SIGN (DCN46 mAb). (B) Control staining of fixed Raji-DCSIGN cells with the lipophilic dye, DiI under TIR illumination. (C) Addition of 580 kDa FITC-dextran to the medium to demonstrate accessibility of the ventral membrane surface of adhered Raji-DCSIGN cells. Data shown are mean intensities of ventral membrane regions from TIR images before and after addition of the reagent. Ventral ROIs were defined as the largest box that could fit within the cell outline as determined from a DIC image. (D) Control stainings of fixed Raji-DCSIGN cells for membrane-associated proteins, CD46 and CD59. These images were collected in TIRF mode to show only material within ~150 nm of the glass substrate. (E) A fixed MDDC stained for DC-SIGN (DCN46 mAb) and visualized by TIR microscopy. (F) 3D projection images to show the dorsolateral membrane distribution of DC-SIGN on fixed Raji-DCSIGN cells as obtained from a deconvoluted z-stack (step=200 nm) of epifluorescence images. (G) DC-SIGN imaged on the dorsal lamellar membrane of a fixed MDDC in a single epifluorescence image focused 2 μm above the coverslip with edge-region detail expanded as indicated. (H) A fixed MDDC imaged for morphology in DIC and for DC-SIGN distribution by deconvolution of a z-stack of epifluorescence images (step=200 nm). Arrows denote active leading edge membrane regions enriched in DC-SIGN. 3D projections are shown as views from 90° (xy plane) and 0° (from the left side of the cell, yz plane). Scale bars, 10 μm.

Images of fluorescence focused on the dorsal lamellar membrane were analyzed to quantify colocalization of DC-SIGN and endocytosis marker signals at various locations between the leading edge and perinuclear zone (Fig. 4A). Consistent with the hypothesis described above, we observed many DC-SIGN clusters at the leading edge of the cells and quantitative analysis of colocalization revealed that these leading edge clusters exhibited little coincidence with the endocytosis marker (Fig. 4B). However, at medial locations in the lamella of dendritic cells, significantly greater colocalization was evident (edge versus medial, P<0.05), suggesting that DC-SIGN clusters were internalized at locations posterior to the leading edge of the lamella. The quantitative colocalization of DC-SIGN and endocytosis marker increased even further in the perinuclear zone (edge versus perinuclear, P<0.001). It is important to note that endocytic events without DC-SIGN were present in our images (Fig. 4A and data not shown) showing that this technique provides a sensitive measure of DC-SIGN internalization. We calculated the minimum distances between the centroid of each DC-SIGN cluster

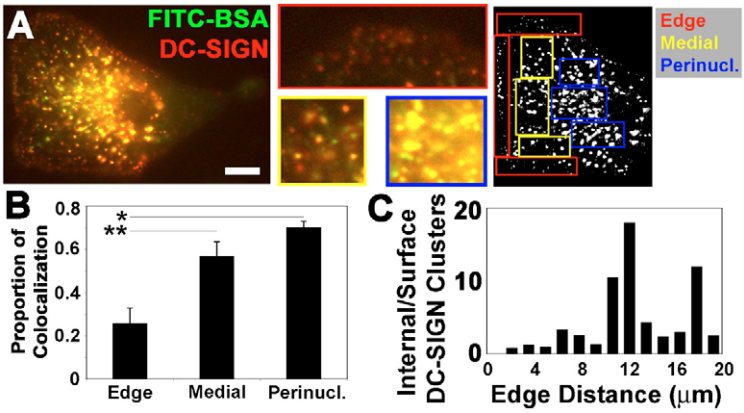

Fig. 4. (A) Colocalization of internalized FITC-BSA and Alexa-Fluor-568 anti-DC-SIGN F(ab) in a MDDC (scale bar, 10 μm). Representative details of edge (red frame), medial zone (yellow frame), and perinuclear zone regions (blue frame) show non-internalized and internalized DC-SIGN. Three regions in each category (shown by red, yellow and blue boxes) were chosen for quantitative colocalization analysis. (B) Proportion of colocalization of DC-SIGN and internalized FITC-BSA per region (*t*-test $*P<0.001$; $**P<0.05$). (C) Histogram of the ratio of internalized clusters versus surface clusters as a function of distance from the edge of the cell. This analysis is representative of four independent experiments.

and the leading edge of the cell, and grouped the data into cluster-to-edge distances for surface DC-SIGN and internalized DC-SIGN. These data are presented as the ratio of internalized DC-SIGN to surface DC-SIGN as a function of cluster-to-edge distance (Fig. 4C). Data from the perinuclear zone were excluded from analysis. On average, internalized DC-SIGN was located a greater distance away from the cell edge (internalized DC-SIGN=8.9±5.1 μm; surface DC-SIGN=6.1±5.1 μm; n=269 total clusters). This difference was statistically significant with very high confidence ($P\leqslant0.001$) as measured by Student's *t*-test.

We also observed endocytosis of DC-SIGN clusters in living dendritic cells by confocal microscopy. We briefly stained dendritic cells with anti-DC-SIGN F(ab), bathed the cells in FITC-BSA and imaged a confocal section through the medial lamellar membrane. Regions inside of the cell are dark due to exclusion of dye with the exception of newly formed endocytic vesicles that contain FITC-BSA. Within the cellular regions, red spots indicate surface DC-SIGN, green spots indicate non-DC-SIGN endocytosis and colocalization (yellow) indicates DC-SIGN endocytosis events (Fig. 5A). The leading edge of a dendritic cell (yellow line) and a region exhibiting DC-SIGN endocytosis (blue box) are shown (Fig. 5B,C). In this example, a surface DC-SIGN cluster located approximately 13 μm from the leading edge was internalized (Fig. 5D, supplementary material Movie 3). The fluorescein signal of the cluster increased to a maximum after ~80 seconds and subsequently began to move in a rapid, linear fashion.

Directed lateral transport of DC-SIGN clusters

We reasoned that it should be possible to observe motion of DC-SIGN clusters between the leading edge and zones of potential internalization. Therefore, we examined the movement of leading edge F(ab)-labeled DC-SIGN clusters on the lamella of live immature dendritic cells using video rate-recording and spot-tracking analysis. Many clusters exhibited little mobility while the movies were taken; however, some clusters moved rearwards from the leading edge (Fig. 6A, and supplementary material Movie 4). We pursued more detailed analysis of four examples of directed lateral mobility. Displacement analysis of the positional information from these trajectories was used to objectively classify the behavior of each trajectory based on mean square displacement (MSD) versus time plot (Saxton, 1994). Directed motion of some DC-SIGN clusters was evident from the positive curvature of their MSD versus t plot (Fig. 6B), whereas the remainder did not show this type of inflection and was labeled non-directed lateral mobility.

Even a random walk can generate a trajectory with an apparent directionality. To quantify the probability that the observed rearward motions were not random, we performed Monte Carlo simulations of random trajectories to establish a 95% confidence limit for head-to-tail length for random walks of a given number of steps. A large

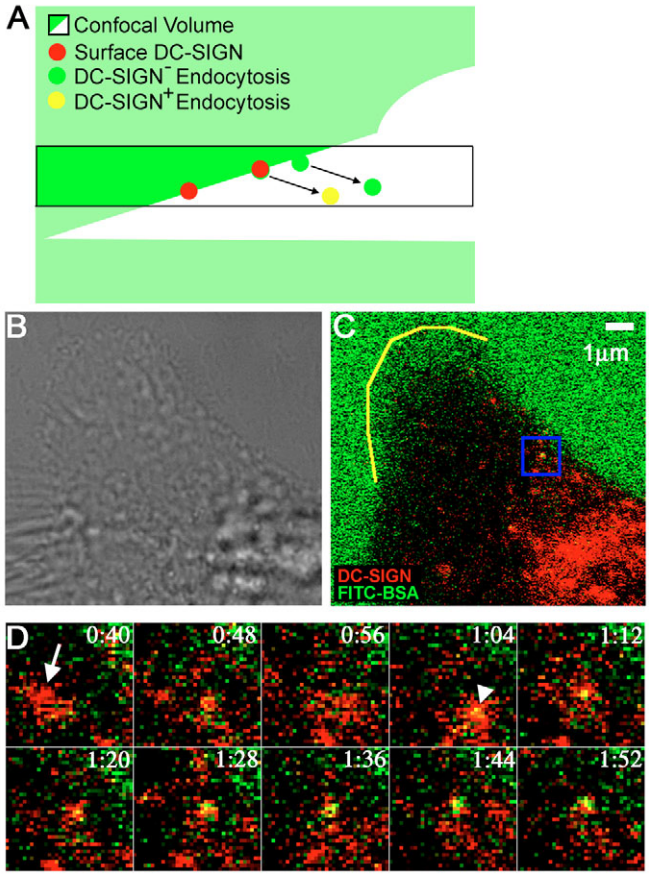

Fig. 5. (A) Schematic representation of the live cell internalization experiment. In dendritic cells stained with anti-DC-SIGN F(ab) (red) and bathed in FITC-BSA as an endocytosis marker (green), a confocal slice containing the medial lamellar membrane was observed. Endocytosis results in a colocalized (yellow) signal. (B) DIC image of the cell under observation. (C) A single frame showing the leading edge of a dendritic cell (yellow line) and a region of interest containing a DC-SIGN cluster that exhibits internalization. (D) A montage of selected frames limited to the region of interest defined in (C) showing the internalization of a DC-SIGN cluster. The arrow shows a surface DC-SIGN cluster before internalization is evident. The arrowhead in a subsequent frame shows the appearance of internalization activity coincident with the surface DC-SIGN cluster.

Journal of Cell Science

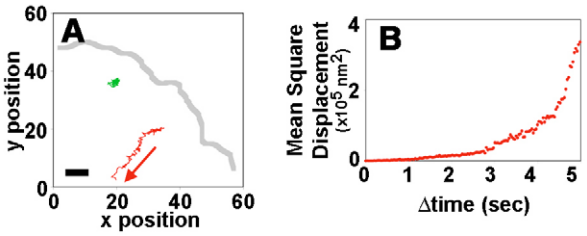

Fig. 6. (A) Representative trajectories of DC-SIGN undergoing directed (red) or non-directed (green) motion relative to the cell edge (gray line). The red arrow denotes overall direction of DC-SIGN displacement for the directed motion trajectory. All trajectories were obtained from live MDDCs stained with anti-DC-SIGN F(ab). Scale bar, 1 μm. (B) Mean square displacement versus time for DC-SIGN trajectories exhibiting directed motion (n=4).

set of random trajectories was generated for comparison with each experimental trajectory, having the same total number and Gaussian step-size distribution as its comparable experimental trajectory. Experimental trajectories were classified as non-random at the stated confidence if their head-to-tail length was greater than the confidence limit (supplementary material Fig. S3). Three of the trajectories identified as directed motion by MSD analysis scored as non-random with 95% confidence and one with 90% confidence (Table 2). The directed motion clusters moved with a speed of 1420±260 nm/second (range: 1149-1756 nm/second).

We also predicted that much of this directed motion occurs in the plane of the plasma membrane. To directly test this prediction, we also used confocal imaging to discriminate surface and internalized DC-SIGN via the staining technique presented previously (Fig. 5). In Fig. 7, a dendritic cell is shown with cell outline (yellow line), internalized DC-SIGN (blue boxes) and mobile surface DC-SIGN spots (arrows) (Fig. 7A,B). Two DC-SIGN clusters, as denoted by white and blue arrows, were clearly non-internalized throughout the experiment and exhibited considerable mobility (supplementary material Movie 5) as shown by their trajectories (Fig. 7C) and selected frames from the Movie (Fig. 7D). It is apparent that some DC-SIGN clusters located on the plasma membrane do exhibit considerable mobility, so the rapid rearward motions observed at higher time resolution above are unlikely to be represent solely transport of endocytic vesicles containing DC-SIGN. The presence of several colocalized spots (Fig. 7C, blue boxes) provides a positive control for detection of internalized DC-SIGN in this experiment.

Discussion

While previous studies of DC-SIGN clustering were concerned with fixed cells (Cambi et al., 2004; Koopman et al., 2004), our study confirms that DC-SIGN clusters are observed in living dendritic cells and cell-line models. The generality of DC-SIGN clustering suggests that the principle underlying this distribution is likely to be receptor self-organization, possibly mediated by lipids (Anderson and Jacobson, 2002) and/or ubiquitously expressed proteins, such as cytoskeletal components or clathrin adaptors. Since our measurements indicate that many of the clusters exceed the diffraction limit in dimension (300 nm FWHM), they could be classified as legitimate nanodomains. However, it is possible that the thresholding procedure excluded very faint clusters some of which could have had very small sizes. Using individual domain FRAP measurements, we have observed that DC-SIGN clusters have remarkably low rates of DC-SIGN exchange with the surrounding membrane, indicating that DC-SIGN clusters in live cells are discrete and stable objects.

Binding is a significant obstacle a virus must first overcome to achieve host cell entry. For instance, HIV-1 virions present little binding area (diameter ~120 nm) and few ligands for host receptor binding (~10 trimers per virion). Indeed, a clustered distribution of DC-SIGN on the membrane has been shown to be necessary for efficient binding of virus-sized particles (Cambi et al., 2004). The importance of avidity for binding interactions is further illustrated by LFA-1 (ITGAL) and ICAM-1 (TICAM1). Inside-out signaling leads to increased clustering of LFA-1 that increases its avidity of interaction with ICAM-1 (Hibbs et al., 1991). Since ICAM-1 can be incorporated into enveloped viruses, LFA-1 can serve as another pathogen receptor where avidity is crucial (Tardif and Tremblay, 2005a; Tardif and Tremblay, 2005b).

Surface DC-SIGN appears to be particularly concentrated at the leading edges of immature dendritic cells. In-vitro-differentiated immature dendritic cells are slowly motile (Burns et al., 2004; van Helden et al., 2006). Nevertheless, the preferential accumulation of DC-SIGN in the leading edge may optimize contact between the dendritic cell and pathogens and/or antigens in sites of infection that enter the DC. Also, the active edges of the dendritic cell lamellipod are known to 'scan' the local environment for efficient particle acquisition (Swetman Andersen et al., 2006); thus, DC-SIGN appears distributed to the active leading edge where it would enhance the antigen-scanning function of the dendritic cell.

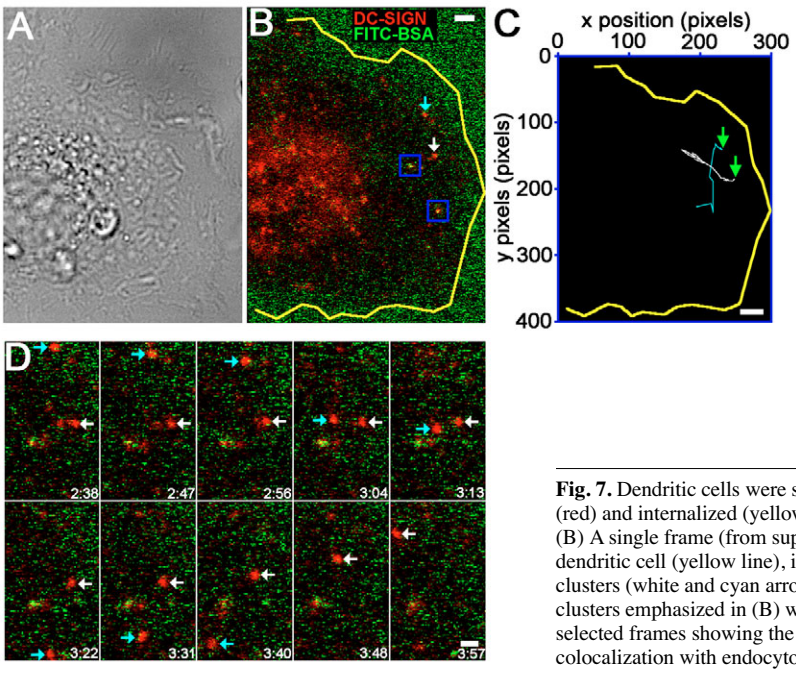

Fig. 7. Dendritic cells were stained and observed as described in Fig. 5 to distinguish surface (red) and internalized (yellow) DC-SIGN. (A) DIC image of the dendritic cell under observation. (B) A single frame (from supplementary material Movie 5) showing the leading edge of the dendritic cell (yellow line), internalized DC-SIGN (blue boxes), and mobile surface DC-SIGN clusters (white and cyan arrows). (C) Trajectories followed by the mobile surface DC-SIGN clusters emphasized in (B) with trajectory start points indicated by green arrows. (D) Montage of selected frames showing the rapid linear mobility of these spots and their continued lack of colocalization with endocytosis marker (FITC-BSA). Scale bars, 1 μm.

Journal of Cell Science

Table 2. Monte Carlo analysis of DC-SIGN trajectory non-randomness

Experimental head-to-tail distance (μm)	90% Confidence limit for non-randomness (μm)	95% Confidence limit for non-randomness (μm)	Confidence
4.82	2.96	3.42	a
8.33	4.94	5.57	a
3.90	3.89	4.54	b
3.59	1.72	2.82	a

a, non-random with 95% confidence; b, non-random with 90% confidence

Little DC-SIGN was observed in the relatively flat ventral membranes of Raji transfectants or within the lamellar membrane of immature dendritic cells. The structural basis of this exclusion is unclear. It is possible that diffusion barriers exist that prevent movement of protein from the dorsolateral to the ventral membrane, or that polarity determining protein complexes may direct the localization of DC-SIGN through as-yet-unknown mechanisms. The functional importance of the ventral exclusion is also not clear; it may relate to DC-SIGN's ability to serve as a cell adhesion molecule but competing DC-SIGN binding to potential glass-adsorbed ligands with excess mannan had no effect on adhesion or motility (data not shown).

We have found that DC-SIGN exists primarily as surface protein at the leading edge of the cell; however, DC-SIGN clusters experience significantly greater internalization in the region of dorsal lamellar membrane medial to the leading edge and perinuclear zone – which we have dubbed the 'medial zone'. Furthermore, we have imaged internalization of surface DC-SIGN clusters in live dendritic cells from this medial zone. The findings that DC-SIGN was enriched at the leading edge and preferentially internalized in the medial zone prompted us to predict lateral transport of DC-SIGN between these two regions (see below). The internalization of DC-SIGN clusters is important for antigen processing and pathogen entry.

Our data show that DC-SIGN clusters are rapidly internalized. This result is consistent with a previous report of active uptake of mannosylated BSA by DC-SIGN and recycling of the receptor (Guo et al., 2004). HIV-1 internalized by DC-SIGN localizes predominantly to non-lysosomal compartments with a pH of 5.0-5.5 within 15 minutes post internalization (Engering et al., 2002; Kwon et al., 2002). It is reasonable to presume that DC-SIGN is recycled while virions are retained in these non-degradative compartments, but further detailed studies are required to fully understand lateral mobility, vesicular trafficking and recycling of DC-SIGN in immature dendritic cells.

Our results demonstrate that some DC-SIGN clusters appear to move in a confined manner whereas others move rapidly. We proposed that these rapid motions represent rearward transport in the plane of the membrane towards the medial lamella prior to endocytosis. An alternative interpretation is that rapidly moving clusters are internalized vesicles that contain DC-SIGN and undergo transport along microtubules. Our live cell imaging of DC-SIGN together with a marker of endocytosis shows that non-internalized DC-SIGN does experience rapid lateral mobility in the membrane. This observation supports the former interpretation that DC-SIGN clusters are transported rapidly in the plane of the membrane.

The directed mobility of DC-SIGN clusters is likely to be the result of motor-protein-driven transport. This mechanism agrees well with the highly linear nature of the directed motion trajectories. In vitro assays have shown that myosin can move along actin filaments at a speed of 3-4 μm/second (Kron and Spudich, 1986). Kinesin velocities reported in vitro have ranged from 0.4-3.8 μm/second (Steinberg and Schliwa, 1996; Vale et al., 1985), and similar measurements with dynein revealed a range of translocation velocities from ~1-10 μm/second (Hamasaki et al., 1995; Vale et al., 1992; Vale and Toyoshima, 1989). Peroxisomes are transported on microtubules in live cells at 1 μm/second (Hamasaki et al., 1995; Vale et al., 1992; Vale and Toyoshima, 1989), and mitochondrial transport on microtubules can reach speeds of 15 μm/second (Hamasaki et al., 1995; Vale et al., 1992; Vale and Toyoshima, 1989). Likewise, unbudded patches of clathrin have been reported to move at ~1 μm/ second in the plasma membrane (Rappoport et al., 2003). These velocities of lateral motion are similar to the velocities measured for DC-SIGN clusters exhibiting directed motion. A retrograde flow of actin has been described in motile cells that sweeps both actin and patches of membrane proteins on the cell surface from the leading edge of the cell rearward (Holifield et al., 1990; Holifield and Jacobson, 1991). However, the velocity of retrograde flow is 10-50 nm/second (Berg and Cheney, 2002; Falk et al., 2004; Mallavarapu and Mitchison, 1999), which is approximately two

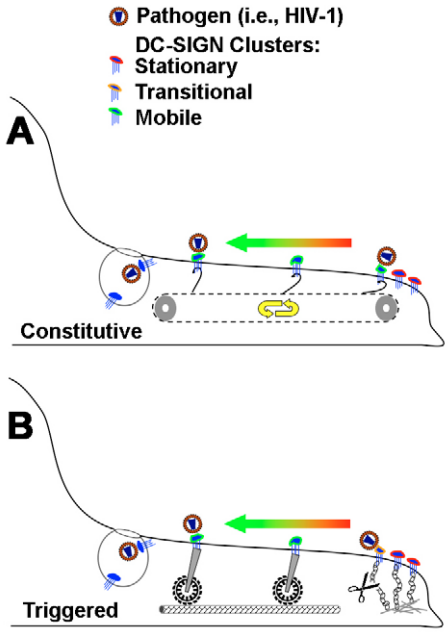

Fig. 8. Two hypothetical models of DC-SIGN cluster rearward motion. (A) The constitutive transport model. DC-SIGN clusters (red border) constitutively leave the leading edge and cycle back (green border) to zones of internalization. Pathogen would be passively transported on structures undergoing this cycling. (B) The triggered transport model. DC-SIGN clusters are caught at the leading edge (red border) and must be liberated (orange border) prior to rearward transport (green border). In this model, pathogen binding would influence the probability of rearward transport of a cluster by affecting its release at the leading edge.

Journal of Cell Science

orders of magnitude slower than the velocity we have observed for the directed mobility of DC-SIGN clusters. Therefore, it seems unlikely these mobilities represent direct coupling of DC-SIGN clusters to the retrograde actin flow; however, a mechanism in which a rearward directed motor 'piggybacks' on the retrograde actin flow remains possible.

In HIV biology, it has been proposed that delivery of HIV-1 to intracellular compartments via DC-SIGN protects the virions from humoral immunity and allows later transfer to T cells for CD4-mediated infection (Piguet and Sattentau, 2004; Kwon et al., 2002; Geijtenbeek et al., 2000). The necessity of DC-SIGN for infection in trans as well as the in vivo relevance of immature dendritic cells to HIV dissemination via this route has been reevaluated recently. DC-SIGN knockdown and blocking ligands are poor inhibitors of in vitro HIV-1 transmission to T cells via human dendritic cells; however, these approaches do significantly attenuate infection in trans when Raji-DCSIGN cell lines are used as donor cells in T cell co-cultures (Boggiano et al., 2007; Granelli-Piperno et al., 2005). C-type lectin receptors on dendritic cells may be redundant, so abrogation of the DC-SIGN trans infection pathway could be compensated by various other lectins in dendritic cells. Raji-DCSIGN cells may be less capable of providing this lectin redundancy, thus explaining their greater dependence on DC-SIGN for infection in trans. Additionally, questions have arisen regarding the expression of DC-SIGN by relevant dendritic cell populations in vivo and their exposure to pathogens (Hladik et al., 2007; Wu and KewalRamani, 2006). Subepithelial DC-SIGN$^+$ DC exist in human vaginal and ileal mucosae, but might not be accessible to HIV unless the epithelium was disrupted (Jameson et al., 2002). DC-SIGN$^+$ DC present throughout the human rectal mucosa may be more accessible to virions, so the possibility remains that dendritic-cell-mediated in trans infection might depend upon tissue integrity and the site of infection.

It is important to understand the lateral mobility of DC-SIGN clusters in their basal state for comparison with cargo-loaded clusters. When a pathogen binds to a cluster of DC-SIGN it must exploit the internalization of DC-SIGN for host cell entry, or in the case of HIV, subsequent delivery to T cells in trans. We suggest two hypothetical models that describe this interaction and its effects on cluster mobility and internalization (Fig. 8). In the constitutive transport model, the virion attaches to a cluster followed by rearward transport and endocytosis following a constitutive pattern of receptor transport. Our observations of unloaded cluster mobility and endocytosis suggest that this model is possible. In the triggered transport model, surface DC-SIGN clusters are retained at the leading edge and released at some frequency to be dragged rearwards. In this model, binding of pathogen to DC-SIGN clusters increases the probability of transition from confined motion at the leading edge to a directed mode of motion for transport, thereby making the internalization of virions more efficient. This model is quite plausible given reports of signaling downstream of DC-SIGN ligation (Caparros et al., 2006; Hodges et al., 2007) and will be tested in future studies.

Materials and Methods

Cell lines

The Raji-DCSIGN and MX-DCSIGN cell lines were obtained from the NIH AIDS Research and Reference Reagent Program (http://www.aidsreagent.org/) and were propagated using the recommended medium.

Monocyte-derived dendritic cells (MDDCs)

Peripheral blood mononuclear cells were isolated from human whole blood freshly drawn from healthy volunteers and centrifuged over a Ficoll gradient (Amersham Biosciences, Uppsala, Sweden). Monocytes were separated by adherence to tissue culture flasks. Immature dendritic cells were prepared by treatment of monocytes with 500 U/ml human IL-4 and 800 U/ml human GM-CSF (Peprotech, Rocky Hill, NJ) in RPMI-1640 medium with 10% FBS in glass-bottom MatTek dishes (MatTek Corp., Ashland, MA). Blood was drawn in accordance with a human subjects research protocol approved by the UNC at Chapel Hill Biomedical IRB.

Fluorescent reagents

Fixed cell specimens were stained for DC-SIGN expression with the anti-human DC-SIGN (DCN46), CD46 (E4.3) and CD59 (H19) mAbs (BD Bioscience, San Jose, CA). Primary antibodies were labeled with Alexa-Fluor-488-conjugated anti-mouse IgG secondary antibody (Invitrogen, Carlsbad, CA). FITC-conjugated 580 kDa dextran and DiI-C18 were obtained from Sigma-Aldrich (St Louis, MO).

Anti-human DC-SIGN F(ab) antibodies were derived from DC6 (6B1-2) IgG (gift of Robert Doms, University of Pennsylvania) using digestion with immobilized papain (Pierce Biotechnology, Rockford, IL) according to manufacturers instructions. Protein electrophoresis prior to use confirmed the completeness of digestion. These DC6 F(ab) were conjugated to Alexa-Fluor-568 using a kit obtained from Invitrogen.

Microscopy

Epifluorescence imaging was performed on an Olympus IX81 inverted microscope with a 60×, 1.4 NA objective lens and stage with *z*-axis stepper motor (Olympus, Center Valley, PA). A 37°C, CO_2-controlled culture dish heater (Warner Instruments) was used for live cell imaging. Epifluorescence illumination was accomplished using a 100 W Hg arc lamp attenuated by a 0.6 neutral density filter for low-light movie acquisition. Objective-based TIR illumination (Olympus) utilized a 25 mW Ar ion laser (Melles Griot, Carlsbad, CA). Filters and dichroic mirrors (Chroma, Rockingham, VT) for Alexa-Fluor-488 imaging were as follows: excitation, 488/10; emission, 535/25; dichroic, 475/25. Filters and dichroic mirrors (Chroma) for Alexa Fluor-568 imaging were as follows: excitation, 535/50; emission, 605/40; dichroic, 530/20. Still images were captured using an air-cooled SensiCam QE CCD camera (Cooke Corp., Romulus, MI) driven by Metamorph (Molecular Devices/Meta Imaging, Downingtown, PA). Moving images were obtained with a cooled, intensified Stanford Photonics (Palo Alto, CA) XR/Mega-10Z ICCD camera at 30 Hz recording speed using the QED In Vivo software package.

Laser scanning confocal imaging was performed on a Zeiss 510 Meta inverted microscope equipped with a live cell chamber. Samples were illuminated with 488 nm and 543 nm lines from a 30 mW Ar ion laser and a 1 mW He-Ne Laser. Filters and dichroic elements were as follows: main dichroic, UV/488/543/633; fluorescein emission filter, LP505; Alexa-Fluor-568 emission filter, LP560. Data were collected in non-interlaced, descanned mode with multitracking (by frame) and no averaging.

Deconvolution of *z*-stacks

Epifluorescence image stacks were collected at 200-nm *z*-step size. Stacks were deconvoluted with the nearest-neighbors algorithm using the Slidebook software package (Intelligent Imaging Innovations Inc., Santa Monica, CA).

DC-SIGN/DiI ratiometric imaging

Fixed dendritic cells were stained using mAb DCN46 plus Alexa-Fluor-488-labeled secondary Ab as well as DiI (C18; 1 μg/ml) and imaged in epifluorescence mode. The extent of bleed-through between these dyes into the inappropriate channels was determined from single stained specimens, and empirical correction factors were obtained to permit subtraction of the bleed-through signal in each channel of the dual-stained specimen images. The ratio of the two bleed-corrected images was taken by dividing the DC-SIGN image by the DiI image and scaling by a factor of 100. For radial mean DC-SIGN/DiI ratio analysis, the cell edge was determined from the DiI image and at least nine radii (single-pixel width) were drawn from a single, central point in the perinuclear zone to the leading edge at regularly spaced intervals. The averaged ratios along these radii were displayed relative to distance from the edge.

DC-SIGN-cluster size distribution

NIH 3T3 cells expressing DC-SIGN were fixed, labeled with Alexa-Fluor-488-conjugated DC6 F(ab)s, and imaged as described above. Complementary images were acquired for ~20-nm diameter streptavidin-conjugated quantum dots emitting at 605 nm (Quantum Dot Corp., Hayward, CA), 200-nm diameter and 500-nm diameter fluorescent beads (Molecular Probes, Eugene, OR), and aggregates of 200-nm diameter beads (produced by biotinylating amine-modified beads followed by streptavidin mediated crosslinking) adhered to glass coverslips. The pixel size in the sample plane was 108×108 nm. According to the manufacturer, the true mean diameter was 216 nm for the nominally 200-nm beads and 431 nm for the nominally 500-nm beads.

For all images, peaks were identified by binarizing the image at the global mean of the image minus one standard deviation. Peak positions were identified using the 'Analyze Particles' routine in the software package ImageJ which returned a list of centroids for spots meeting the condition $9 \leqslant$ area $\leqslant 144$. For each image, peak positions and raw data were imported into Mathematica for subsequent analysis. In

Journal of Cell Science

this software package, for each peak in each image, a 13×13 pixel array in which the peak position was centered was defined. Each 269-point array was curve-fit to the following two-dimensional Gaussian function:

$$F(i,j) = a\exp\left[-\frac{(i-b)^2 + (j-c)^2}{2h^2}\right] + d\,, \quad (5)$$

in which $1 \leqslant (i,j) \leqslant 13$ are the pixel positions, a is the maximum intensity above background, b and c are the peak centers, d is the local background, and h describes the peak width. For accurate curvefitting in Mathematica, the starting parameters are important. They were as follows: parameter a, the difference between the maximum and minimum intensity in the 169-pixel array; parameters b and c, 7; parameter d, the minimum intensity in the 169-pixel array; h, 2 pixels.

For each image, after initial curve-fitting, a screen was applied in which some peaks were rejected from further analysis. This screen was composed of rejecting peaks so close to the image boundary that a 13×13 pixel array could not be defined, in addition to the following conditions: a >0, 4< b <10, 4< c <10, d >0, a + d<3500. The last condition provided a very conservative guard against possible camera saturation for a given peak. This screen, overall, rejected 9% of the peaks for DC-SIGN clusters, 5% of the peaks for quantum dots, 10% of the peaks for 200-nm beads, 45% of the peaks for 500-nm beads, and 21% of the peaks for aggregates of 200-nm beads.

DC-SIGN endocytosis assays

DC-SIGN was labeled in live dendritic cells using the Alexa-Fluor-568 labeled F(ab) reagent described above by staining at 50 μg/ml for 3 minutes at 37°C. For endocytosis experiments presented in Fig. 4, FITC-BSA was present at 0.2 mg/ml during this staining period followed by washing and immediate fixation in 4% paraformaldehyde. For live cell endocytosis imaged by confocal microscopy, FITC-BSA was present during the staining (0.2 mg/ml) followed by washing to remove F(ab) and was subsequently added again at the start of image acquisition at the same concentration.

Internalization analysis using fixed dendritic cells

All image processing, except spot tracking (see below), was done in ImageJ. The identical regions of interest were selected in both red (DC-SIGN label) and green (FITC-BSA) channel images. These ROIs were binarized with a threshold equal to their mean fluorescence intensity. The binarized image was submitted as input for the particle analyzer module with a minimal spot size of 3×3 pixels to exclude random noise. This procedure generated a binarized mask of all identified spots in both red and green images and an accompanying list of spot centroids. Colocalized spots were identified by the logical operation (Red image) AND (Green image), and non-colocalized DC-SIGN was identified by the operation (Red Image) minus (Colocalized spots image). Probability of colocalization was calculated for each processed region of interest (ROI) as the total number of colocalized pixels per total number of red pixels. To determine the spot to edge distance, a cell outline was manually defined and the minimum distance from each identified spot centroid to a cell outline pixel was calculated. These distances were grouped according to the identification of the spots as colocalized or non-colocalized. Comparison between ROIs in edge, medial and perinuclear regions was done using Student's t-test.

Spot tracking

Tracking of DC-SIGN spots in 30 Hz movies was accomplished with the Metamorph (Molecular Devices) Track Objects function using the Threshold Result algorithm (50% size match criterion). The spot of interest was defined manually by a 6×6 pixel region in the first frame and tracked automatically thereafter with a 10×10-pixel search area.

Fluorescence recovery after photobleaching

Live cells were stained with Alexa-Fluor-568 labeled F(ab) reagent described above by staining at 50 μg/ml for 3 minutes at 37°C. Small regions of the cell containing individual DC-SIGN clusters were bleached using the 543 nm He-Ne laser line at maximum power. Bleaching was carried to ~50% completion to allow post-bleach tracking of the effected cluster(s). The bleached cluster was tracked using a custom designed MatLab program that allows collection of fluorescence recovery information from a region of interest that defines the DC-SIGN cluster and that moves according to the centroid of the effected cluster. Tracking algorithms were obtained from the MatLab Particle Tracking Code Repository (www.seas.harvard.edu/projects/weitzlab/matlab). Mobile fraction (M_f) was calculated as follows:

$$M_f(\%) = \frac{I_{final} - I_{post}}{I_{pre} - I_{post}} \times 100\,, \quad (6)$$

where I represents the integrated cluster intensity for the pre-bleach period (averaged over all pre-bleach frames), the first post-bleach frame, or the final period (averaged over the final ten frames).

Monte Carlo simulations

Simulations were conducted with custom software written in MatLab. Briefly, the step-size distribution was determined for each experimental trajectory based on its positional information. Simulated random trajectories were generated with the same total number of steps and same Gaussian distribution of step sizes. At each step, the heading was chosen according to an even random distribution over 0-2π radians and was independent of the previous step. One thousand independent simulated trajectories were generated for each experimental trajectory, and head-to-tail distances were calculated from the positions of the origin and endpoint. The head-to-tail distances that were ⩾90% or 95% of the simulated trajectory head-to-tail distances were defined as the respective confidence limits. These confidence limits were compared with the head-to-tail distances of experimental trajectories to determine whether the experimental trajectory could be distinguished from a random walk with the stated confidence.

The authors thank Yun Chen, Zenon Rajfur and Gabriel Weinreb for helpful discussions related to the Monte Carlo and quantitative colocalization analyses. We also appreciate assistance from Shawn Janeiro relating to cluster FRAP analysis. A.K.N. was supported by postdoctoral fellowships from the Lineberger Comprehensive Cancer Center (T32CA09156) and the NIH (F32AI71900). This research was funded by NIH (R01GM041402) awarded to K.J. and N.L.T.

References

Anderson, R. G. and Jacobson, K. (2002). A role for lipid shells in targeting proteins to caveolae, rafts, and other lipid domains. *Science* **296**, 1821-1825.

Banchereau, J. and Steinman, R. M. (1998). Dendritic cells and the control of immunity. *Nature* **392**, 245-252.

Berg, J. S. and Cheney, R. E. (2002). Myosin-X is an unconventional myosin that undergoes intrafilopodial motility. *Nat. Cell Biol.* **4**, 246-250.

Boggiano, C., Manel, N. and Littman, D. R. (2007). Dendritic cell-mediated trans-enhancement of human immunodeficiency virus type 1 infectivity is independent of DC-SIGN. *J. Virol.* **81**, 2519-2523.

Burns, S., Hardy, S. J., Buddle, J., Yong, K. L., Jones, G. E. and Thrasher, A. J. (2004). Maturation of DC is associated with changes in motile characteristics and adherence. *Cell Motil. Cytoskeleton* **57**, 118-132.

Cambi, A., de Lange, F., van Maarseveen, N. M., Nijhuis, M., Joosten, B., van Dijk, E. M., de Bakker, B. I., Fransen, J. A., Bovee-Geurts, P. H., van Leeuwen, F. N. et al. (2004). Microdomains of the C-type lectin DC-SIGN are portals for virus entry into dendritic cells. *J. Cell Biol.* **164**, 145-155.

Cambi, A., Koopman, M. and Figdor, C. G. (2005). How C-type lectins detect pathogens. *Cell. Microbiol* **7**, 481-488.

Caparros, E., Munoz, P., Sierra-Filardi, E., Serrano-Gomez, D., Puig-Kroger, A., Rodriguez-Fernandez, J. L., Mellado, M., Sancho, J., Zubiaur, M. and Corbi, A. L. (2006). DC-SIGN ligation on dendritic cells results in ERK and PI3K activation and modulates cytokine production. *Blood* **107**, 3950-3958.

Engering, A., Geijtenbeek, T. B., van Vliet, S. J., Wijers, M., van Liempt, E., Demaurex, N., Lanzavecchia, A., Fransen, J., Figdor, C. G., Piguet, V. et al. (2002). The dendritic cell-specific adhesion receptor DC-SIGN internalizes antigen for presentation to T cells. *J. Immunol.* **168**, 2118-2126.

Falk, J., Thoumine, O., Dequidt, C., Choquet, D. and Faivre-Sarrailh, C. (2004). NrCAM coupling to the cytoskeleton depends on multiple protein domains and partitioning into lipid rafts. *Mol. Biol. Cell* **15**, 4695-4709.

Frankel, A. D. and Young, J. A. (1998). HIV-1: fifteen proteins and an RNA. *Annu. Rev. Biochem.* **67**, 1-25.

Geijtenbeek, T. B., Kwon, D. S., Torensma, R., van Vliet, S. J., van Duijnhoven, G. C., Middel, J., Cornelissen, I. L., Nottet, H. S., KewalRamani, V. N., Littman, D. R. et al. (2000). DC-SIGN, a dendritic cell-specific HIV-1-binding protein that enhances trans-infection of T cells. *Cell* **100**, 587-597.

Geijtenbeek, T. B., Engering, A. and Van Kooyk, Y. (2002). DC-SIGN, a C-type lectin on dendritic cells that unveils many aspects of dendritic cell biology. *J. Leukoc. Biol.* **71**, 921-931.

Granelli-Piperno, A., Pritsker, A., Pack, M., Shimeliovich, I., Arrighi, J. F., Park, C. G., Trumpfheller, C., Piguet, V., Moran, T. M. and Steinman, R. M. (2005). Dendritic cell-specific intercellular adhesion molecule 3-grabbing nonintegrin/CD209 is abundant on macrophages in the normal human lymph node and is not required for dendritic cell stimulation of the mixed leukocyte reaction. *J. Immunol.* **175**, 4265-4273.

Guo, Y., Feinberg, H., Conroy, E., Mitchell, D. A., Alvarez, R., Blixt, O., Taylor, M. E., Weis, W. I. and Drickamer, K. (2004). Structural basis for distinct ligand-binding and targeting properties of the receptors DC-SIGN and DC-SIGNR. *Nat. Struct. Mol. Biol.* **11**, 591-598.

Hamasaki, T., Holwill, M. E., Barkalow, K. and Satir, P. (1995). Mechanochemical aspects of axonemal dynein activity studied by in vitro microtubule translocation. *Biophys. J.* **69**, 2569-2579.

Hibbs, M. L., Xu, H., Stacker, S. A. and Springer, T. A. (1991). Regulation of adhesion of ICAM-1 by the cytoplasmic domain of LFA-1 integrin beta subunit. *Science* **251**, 1611-1613.

Hladik, F., Sakchalathorn, P., Ballweber, L., Lentz, G., Fialkow, M., Eschenbach, D. and McElrath, M. J. (2007). Initial events in establishing vaginal entry and infection by human immunodeficiency virus type-1. *Immunity* **26**, 257-270.

Hodges, A., Sharrocks, K., Edelmann, M., Baban, D., Moris, A., Schwartz, O., Drakesmith, H., Davies, K., Kessler, B., McMichael, A. et al. (2007). Activation of the lectin DC-SIGN induces an immature dendritic cell phenotype triggering Rho-GTPase activity required for HIV-1 replication. *Nat. Immunol.* **8**, 569-577.

Holifield, B. F. and Jacobson, K. (1991). Mapping trajectories of Pgp-1 membrane protein patches on surfaces of motile fibroblasts reveals a distinct boundary separating capping on the lamella and forward transport on the retracting tail. *J. Cell Sci.* **98**, 191-203.

Holifield, B. F., Ishihara, A. and Jacobson, K. (1990). Comparative behavior of membrane protein-antibody complexes on motile fibroblasts: implications for a mechanism of capping. *J. Cell Biol.* **111**, 2499-2512.

Jameson, B., Baribaud, F., Pohlmann, S., Ghavimi, D., Mortari, F., Doms, R. W. and Iwasaki, A. (2002). Expression of DC-SIGN by dendritic cells of intestinal and genital mucosae in humans and rhesus macaques. *J. Virol.* **76**, 1866-1875.

Koopman, M., Cambi, A., de Bakker, B. I., Joosten, B., Figdor, C. G., van Hulst, N. F. and Garcia-Parajo, M. F. (2004). Near-field scanning optical microscopy in liquid for high resolution single molecule detection on dendritic cells. *FEBS Lett.* **573**, 6-10.

Kron, S. J. and Spudich, J. A. (1986). Fluorescent actin filaments move on myosin fixed to a glass surface. *Proc. Natl. Acad. Sci. USA* **83**, 6272-6276.

Kwon, D. S., Gregorio, G., Bitton, N., Hendrickson, W. A. and Littman, D. R. (2002). DC-SIGN-mediated internalization of HIV is required for trans-enhancement of T cell infection. *Immunity* **16**, 135-144.

Lakadamyali, M., Rust, M. J., Babcock, H. P. and Zhuang, X. (2003). Visualizing infection of individual influenza viruses. *Proc. Natl. Acad. Sci. USA* **100**, 9280-9285.

Lehmann, M. J., Sherer, N. M., Marks, C. B., Pypaert, M. and Mothes, W. (2005). Actin- and myosin-driven movement of viruses along filopodia precedes their entry into cells. *J. Cell Biol.* **170**, 317-325.

Mallavarapu, A. and Mitchison, T. (1999). Regulated actin cytoskeleton assembly at filopodium tips controls their extension and retraction. *J. Cell Biol.* **146**, 1097-1106.

Piguet, V. and Sattentau, Q. (2004). Dangerous liaisons at the virological synapse. *J. Clin. Invest.* **114**, 605-610.

Rappoport, J. Z., Taha, B. W. and Simon, S. M. (2003). Movement of plasma-membrane-associated clathrin spots along the microtubule cytoskeleton. *Traffic* **4**, 460-467.

Ray, N. and Doms, R. W. (2006). HIV-1 coreceptors and their inhibitors. *Curr. Top. Microbiol. Immunol.* **303**, 97-120.

Saxton, M. J. (1994). Single-particle tracking: models of directed transport. *Biophys. J.* **67**, 2110-2119.

Steinberg, G. and Schliwa, M. (1996). Characterization of the biophysical and motility properties of kinesin from the fungus Neurospora crassa. *J. Biol. Chem.* **271**, 7516-7521.

Swetman Andersen, C. A., Handley, M., Pollara, G., Ridley, A. J., Katz, D. R. and Chain, B. M. (2006). beta1-Integrins determine the dendritic morphology which enhances DC-SIGN-mediated particle capture by dendritic cells. *Int. Immunol.* **18**, 1295-1303.

Tardif, M. R. and Tremblay, M. J. (2005a). LFA-1 is a key determinant for preferential infection of memory CD4+ T cells by human immunodeficiency virus type 1. *J. Virol.* **79**, 13714-13724.

Tardif, M. R. and Tremblay, M. J. (2005b). Regulation of LFA-1 activity through cytoskeleton remodeling and signaling components modulates the efficiency of HIV type-1 entry in activated CD4+ T lymphocytes. *J. Immunol.* **175**, 926-935.

Theriot, J. A. and Mitchison, T. J. (1992). Comparison of actin and cell surface dynamics in motile fibroblasts. *J. Cell Biol.* **119**, 367-377.

Vale, R. D. and Toyoshima, Y. Y. (1989). Microtubule translocation properties of intact and proteolytically digested dyneins from Tetrahymena cilia. *J. Cell Biol.* **108**, 2327-2334.

Vale, R. D., Reese, T. S. and Sheetz, M. P. (1985). Identification of a novel force-generating protein, kinesin, involved in microtubule-based motility. *Cell* **42**, 39-50.

Vale, R. D., Malik, F. and Brown, D. (1992). Directional instability of microtubule transport in the presence of kinesin and dynein, two opposite polarity motor proteins. *J. Cell Biol.* **119**, 1589-1596.

van Helden, S. F., Krooshoop, D. J., Broers, K. C., Raymakers, R. A., Figdor, C. G. and van Leeuwen, F. N. (2006). A critical role for prostaglandin E2 in podosome dissolution and induction of high-speed migration during dendritic cell maturation. *J. Immunol.* **177**, 1567-1574.

Weis, W. I., Taylor, M. E. and Drickamer, K. (1998). The C-type lectin superfamily in the immune system. *Immunol. Rev.* **163**, 19-34.

Wu, L. and KewalRamani, V. N. (2006). Dendritic-cell interactions with HIV: infection and viral dissemination. *Nat. Rev. Immunol.* **6**, 859-868.

Journal of Cell Science